NANO LETTERS

pubs.acs.org/NanoLett Letter

Generation of Tin-Vacancy Centers in Diamond via Shallow Ion Implantation and Subsequent Diamond Overgrowth

Alison E. Rugar,* Haiyu Lu, Constantin Dory, Shuo Sun, Patrick J. McQuade, Zhi-Xun Shen, Nicholas A. Melosh, and Jelena Vučković

Cite This: https://dx.doi.org/10.1021/acs.nanolett.9b04495 Read Online

ACCESS | Metrics & More | Article Recommendations | Supporting Information

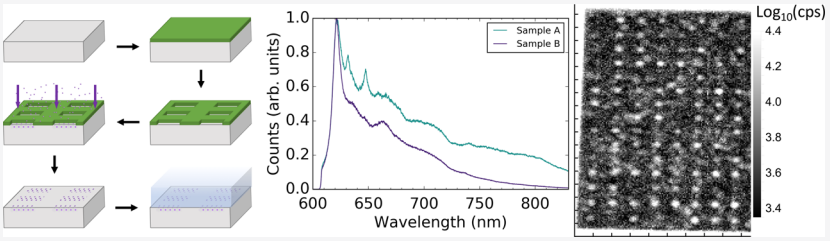

ABSTRACT: Group IV color centers in diamond have garnered great interest for their potential as optically active solid-state spin qubits. The future utilization of such emitters requires the development of precise site-controlled emitter generation techniques that are compatible with high-quality nanophotonic devices. This task is more challenging for color centers with large group IV impurity atoms, which are otherwise promising because of their predicted long spin coherence times without a dilution refrigerator. For example, when applied to the negatively charged tin-vacancy (SnV^-) center, conventional site-controlled color center generation methods either damage the diamond surface or yield bulk spectra with unexplained features. Here we demonstrate a novel method to generate site-controlled SnV^- centers with clean bulk spectra. We shallowly implant Sn ions through a thin implantation mask and subsequently grow a layer of diamond via chemical vapor deposition. This method can be extended to other color centers and integrated with quantum nanophotonic device fabrication.

KEYWORDS: *diamond color centers, tin-vacancy center, CVD growth, ion implantation*

Group IV color centers in diamond have emerged as promising candidates for optically active, solid-state spin qubits.[1−4] These color centers are composed of a split vacancy in the diamond lattice and an interstitial group IV atom. The inversion symmetry of this structure provides group IV color centers with beneficial properties such as insensitivity to electric field fluctuations to first order and high Debye−Waller factors.[5] These color centers also possess long-lived electron spins that can be harnessed as quantum memories.[6−8] All of these characteristics make group IV color centers well suited to interface optical photons in nanophotonic platforms for applications in quantum networks.

An outstanding challenge in implementing these color centers in scalable applications is their generation. The two most common methods of group IV color center generation are ion implantation and synthesis. Ion implantation facilitates the site-controlled generation of color centers by using either a mask[9,10] or a focused ion beam (FIB).[11,12] However, the quality of ion-implanted emitters is often degraded by the large amount of damage introduced during implantation.[4] Synthesis techniques such as high-pressure, high-temperature (HPHT) growth and chemical vapor deposition (CVD) growth often yield higher-quality, more stable emitters with lower inhomogeneous broadening than ion implantation.[13−16] Unfortunately, synthesis techniques do not enable site-controlled generation. A better color center generation method is severely lacking.

Here we introduce a novel method of generating color centers that overcomes the trade-off between site control and surface and emitter quality. We apply this method, which we call shallow ion implantation and growth (SIIG), to generate negatively charged tin-vacancy (SnV^-) centers. Interest in larger group IV atoms such as the SnV^- center has grown because the larger spin−orbit interaction enables longer spin coherence times without requiring dilution refrigerators.[17] However, the issue of generating color centers without significant lattice damage is all the more pertinent to color centers with larger atoms. High-quality SnV^- centers have been generated only with HPHT annealing or growth.[18−20] Of these two methods, only HPHT annealing enables site-controlled color center generation, but it also may damage the diamond surface[21] and thus inhibit subsequent nano-

Received: October 30, 2019
Revised: January 7, 2020
Published: February 7, 2020

https://dx.doi.org/10.1021/acs.nanolett.9b04495
Nano Lett. XXXX, XXX, XXX−XXX

Table 1. Summary of the Fabrication Steps Performed on Each of the Samples Studied

sample	preimplantation steps	implantation conditions	postimplantation steps
A	triacid clean, 500 nm O_2 plasma etch	370 keV, 2×10^{13} cm^{-2}	vacuum anneal 30 min at 800 °C, 30 min at 1100 °C
B	triacid clean, 500 nm O_2 plasma etch, spin on PMMA, e-beam lithography	1 keV, 2×10^{13} cm^{-2}	remove PMMA, H_2 plasma clean, 90 nm MPCVD diamond growth

photonic device fabrication. Ion implantation with vacuum annealing, while compatible with nanophotonic fabrication, produces samples that display bulk photoluminescence (PL) spectra with extraneous peaks.[22,23] With the SIIG method, we demonstrate the site-controlled color center generation of SnV^- centers. We also demonstrate that this method generates high-quality SnV^- centers consistently: the extraneous emission peaks around 631 and 647 nm in the bulk spectra are absent in the SIIG sample. This result, to our knowledge, is unprecedented in the absence of HPHT conditions.

Two samples, named A and B, summarized in Table 1, are studied in this letter. Both samples started as electronic-grade diamond plates from Element Six. The diamond chips were cleaned in a boiling triacid solution (1:1:1 sulfuric/nitric/perchloric acids). An oxygen (O_2) plasma etch was then used to remove 500 nm of diamond. Sample A was implanted at CuttingEdge Ions with $^{120}Sn^+$ ions at 370 keV and 2×10^{13} cm^{-2}. It was then annealed under vacuum ($\sim 10^{-4}$ Torr) at 800 °C for 30 min and 1100 °C for 30 min. Sample A provides a baseline for color center quality to which we compare the results of the SIIG method.

Sample B was prepared via the SIIG method with a patterned implantation mask, as shown schematically in Figure 1. Sample B was spin-coated with ~50 nm of poly(methyl methacrylate) (PMMA, specifically 950 PMMA A2). The PMMA was then patterned via electron-beam (e-beam) lithography in arrays of square holes ranging in side length from 20 to 150 nm. Several 10 μm × 10 μm holes were also patterned for bulk measurements. After the PMMA was developed in an ~5 °C 3:1 solution of isopropanol/water, sample B was sent to CuttingEdge Ions for shallow ion implantation $^{120}Sn^+$ ions at 1 keV with a dose of 2×10^{13} cm^{-2}. The PMMA mask was then removed with Remover PG, and we began the diamond growth procedure. The surface was cleaned with hydrogen (H_2) plasma. Immediately thereafter we grew a nominal 90-nm-thick layer of diamond via microwave-plasma CVD (MPCVD, Seki Diamond Systems SDS 5010) with 300 sccm H_2, 0.5 sccm CH_4, stage temperature of 650 °C, microwave power of 1100 W, and pressure of 23 Torr.

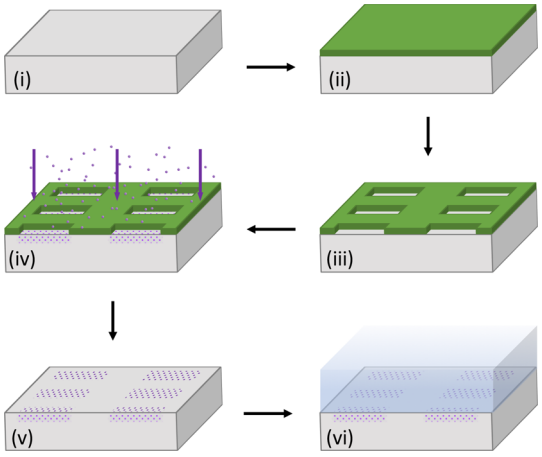

Figure 1. Schematic of the SIIG method of SnV^- center generation used in this letter. (i) Starting with electronic-grade diamond (gray), perform triacid clean and etch at ~500 nm with O_2 plasma; (ii) spin coat at ~50 nm of PMMA (green); (iii) pattern the PMMA via e-beam lithography; (iv) perform 1 keV implantation of $^{120}Sn^+$ ions (purple); (v) remove PMMA with Remover PG; and (vi) clean the surface with H_2 plasma and immediately grow 90 nm of diamond via MPCVD.

By first implanting with low energy, we localize ions and related lattice damage to within ~2 nm of the surface, with lateral and longitudinal straggles of 3 Å, as calculated in stopping and range of ions in matter (SRIM) simulations. The H_2 plasma then removes unwanted sp^2-bonded carbon that may have resulted from implantation damage. Similarly, during the MPCVD growth, sp^2 bonds are removed and new sp^3 bonds are formed, healing and reconstructing the damaged lattice near the surface while incorporating the Sn atoms into the growing diamond lattice to form SnV^- centers. As an added benefit, MPCVD growth enables us to control the depth of the δ-doped layer of Sn ions. We are thus freed of limitations imposed by the maximum implantation energy available and the increased ion straggle expected from higher-energy implantation.

We first compare the average bulk PL spectra of samples A and B acquired at room temperature and 5 K, shown in Figure 2. Although the spectra for both samples display a prominent SnV^- zero-phonon line (ZPL) around 620 nm, they differ significantly in the rest of the measured wavelength range. We

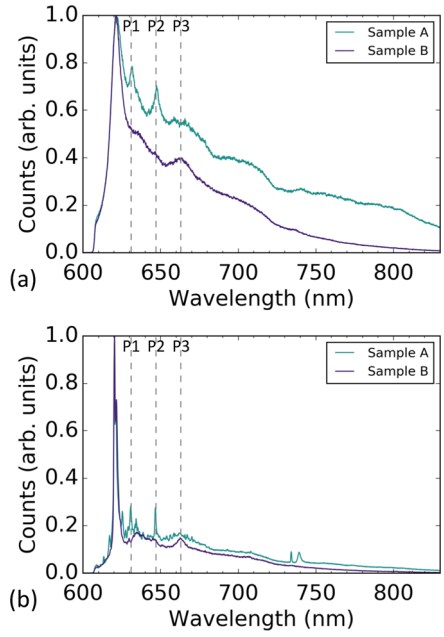

Figure 2. PL spectra from two methods. (a) PL spectra at room temperature for samples A (teal) and B (purple). Gray dashed lines labeled P1, P2, and P3 respectively mark 631, 647, and 663 nm. (b) The same as (a) for samples held at 5 K. Features around 631 and 647 nm are present only in the spectra for sample A.

https://dx.doi.org/10.1021/acs.nanolett.9b04495
Nano Lett. XXXX, XXX, XXX−XXX

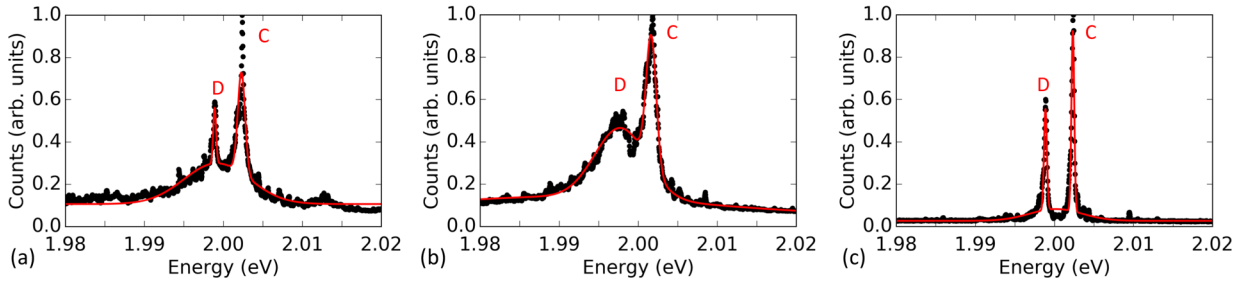

Figure 3. Inhomogeneous broadening. (a) Spectrum of the C and D transitions at 5 K for sample A. The spectrum is an average of four spectra collected via multimode fiber at different spots on the sample. The fit to the data (black dots) is shown in red. (b) The same as (a) for sample B. (c) The same as (a) for an average of spectra collected via multimode fiber at three different spots on a third sample that was made with SIIG with a different initial etch depth and a lower implantation dose.

note three wavelengths around which the two spectra differ: 631, 647, and 663 nm, marked in Figure 2 as P1, P2, and P3, respectively.

Around P1 and P2, peaks are present in the spectra of sample A but not sample B. These peaks have been observed in previous studies of Sn-implanted diamond.[18,24] The suppression of these two peaks as observed in sample B has been previously achieved only through HPHT processing.[18,20] Because sample B never underwent any HPHT process, the SIIG method for forming SnV^- centers is unique from simply annealing an implanted sample.

The origins of the peaks at P1 and P2 are, as yet, unclear. Some argue that because these peaks have been found to disappear under certain conditions, they are not related to the SnV^- center.[20] Under this interpretation, the absence of these peaks in the PL spectrum of sample B indicates that the SIIG method enables the formation of SnV^- centers and mitigates the creation of the defects responsible for the 631 and 647 nm emission. Another interpretation of the 631 nm emission is that it is a quasi-local mode in the phonon sideband of the SnV^- center which is allowed only when the symmetry of the defect center is broken, e.g., via strain.[19,24] Following the argument in ref 19, the disappearance of the 631 nm line in the bulk spectrum for the SIIG method would imply that the SIIG method produces a low-strain, high-quality crystal around the SnV^- centers.

While we currently cannot definitively state the source of the peak at P1, we have investigated in greater detail the origin of the peak at P2. The 647 nm peak, at P2, was previously observed by Iwasaki et al.[18] and Tchernij et al.[24] In previous studies, the 647 nm emission was observed only in Sn-implanted regions[24] and was found to vary in intensity depending on the annealing temperature, ultimately disappearing after an HPHT anneal at 2100 °C and 7.7 GPa.[18] These observations indicate that the 647 nm peak may be from a Sn-related color center that is not the SnV^- center. In the Supporting Information,[25] we present room-temperature and cryogenic spectra exhibiting the 647 nm line when sample A was excited with 632.8 nm laser light, further evidence that the 647 nm peak is not from the SnV^- center.

The third feature at around 663 nm is present in sample A as a broad bump, while it appears in sample B as a narrower peak. The presence of a peak at around 663 nm is consistent with not only the experimental results of Iwasaki et al. after an HPHT anneal[18] and SnV^- centers synthesized via HPHT[20] but also density functional theory (DFT) calculations of the SnV^- spectrum.[17] Upon closer inspection of the cryogenic spectrum shown in Figure 2b, we find that the phonon sideband of sample B holds quite a good qualitative resemblance to that calculated by DFT in ref 17. For example, in addition to the peak at around 663 nm, the spectrum of sample B shares with the DFT-predicted spectrum peaks around 635 and 645 nm. These similarities to DFT calculations indicate that the emission spectrum of sample B is dominated by SnV^- emission. By contrast, the SnV^- PL spectrum of sample A seems to be obscured by additional emission.

Another figure of merit that can be used to characterize the emitter quality is the inhomogeneous broadening. For group IV color centers, inhomogeneous broadening typically comes from variations in strain throughout the sample[26,27] and can therefore serve as an indicator of sample quality after emitter generation. We quantify the inhomogeneous broadening for both samples A and B by averaging PL spectra acquired at four different spots on the sample and fitting Gaussians to the C and D ZPL transitions in the resulting spectra, as shown in Figure 3. To demonstrate how sample preparation can improve inhomogeneous broadening in SIIG samples, a third sample, sample C, is also studied. Sample C was prepared via SIIG but had a deeper initial etch and a lower implantation dose than sample B. More details on the fits and the preparation of sample C can be found in the Supporting Information.[25]

For sample A, the fit to the average ensemble PL reveals full width at half-maximum values (fwhm's) of 263 ± 5 and 105 ± 5 GHz for the C and D transitions, respectively, at 5 K. In sample B, the fwhm's for the average ensemble C and D transitions are broader at 363 ± 4 and 1858 ± 20 GHz, respectively. By contrast, for sample C, the fwhm's in the average ensemble PL are much narrower than those of sample B and are comparable to or narrower than those of sample A: 101 ± 1 and 105 ± 2 GHz for the C and D transitions, respectively. The stark contrast between the broadening observed in samples B and C indicates the importance of sample preparation with the SIIG method and the potential to further reduce the inhomogeneous broadening by optimizing the sample preparation. The narrow distribution of emitters in sample C is promising because it is narrower than that in implanted and vacuum-annealed sample A. Furthermore, the ∼100 GHz inhomogeneous broadening displayed by sample C is narrow enough to be overcome by techniques such as Raman tuning, which has a demonstrated tuning range of 100 GHz for a silicon-vacancy (SiV^-) center.[28,29]

A potential application of the SIIG method of generating SnV^- centers is patterned implantation. By requiring a very low ion implantation energy, this method obviates the need for extremely thick implantation masks which limit the minimum

https://dx.doi.org/10.1021/acs.nanolett.9b04495
Nano Lett. XXXX, XXX, XXX−XXX

achievable hole size[9] or high aspect ratio masks[10] which are quite complicated to fabricate and the efficacy of which is ultimately limited by lateral ion straggle. Instead, we are able to use an ∼50-nm-thick layer of PMMA to stop the implanted ions. We patterned arrays of square holes in the PMMA via e-beam lithography, as described above. In Figure 4, we focus on

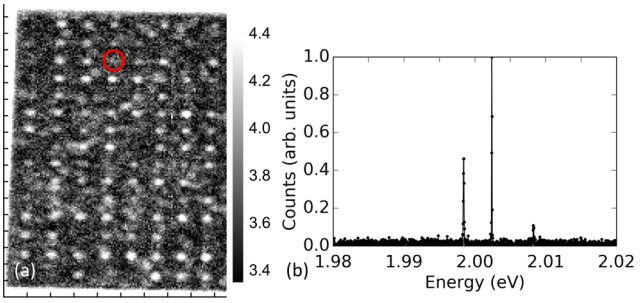

Figure 4. Site-controlled generation of SnV^- centers. (a) PL map resulting from color center generation with a 15-row × 8-column array of 30 nm × 30 nm holes. The color scale bar is $\log_{10}$(counts/s). Ticks on axes are in 1 μm increments. (b) PL spectrum of the SnV^- center located at the site circled in red in (a).

a region that was masked with an array of 30 nm holes. Many (78%) of the holes in the region yielded at least one, or often more, SnV^- center, resulting in an array of SnV^- centers apparent in the PL map of Figure 4(a). From this array, we selected one of the sites, circled in red, that has a small number of SnV^- centers. The PL spectrum measured at 5 K for this site is presented in Figure 4(b). With this array, we estimate the conversion efficiency to be at least 1%. (See the Supporting Information for details.[25])

We have introduced a new method for generating SnV^- centers that yields clean, consistent bulk PL spectra without the need for HPHT processing and that enables the high-precision placement of color centers with a simple mask of PMMA. The use of low-energy ion implantation in the SIIG method significantly reduces the extent of lattice damage, length of ion straggle, and thickness of PMMA required to stop ions. These improvements are key to precisely placing high-quality color centers in arrays. The subsequent MPCVD growth of diamond facilitates SnV^- formation and can be continued arbitrarily to position the δ-doped layer of color centers at the desired depth. The SIIG method may thus be incorporated with existing diamond fabrication techniques[30−34] to precisely place color centers within diamond nanostructures[9,35] for applications in nanophotonics and phononics.

We find that extraneous spectral features typically observed in Sn-implanted samples in the absence of HPHT processing disappear with the SIIG method. This observation indicates that the SIIG method is unique compared to standard implantation and annealing techniques. The SIIG method is also distinct from conventional CVD-based color center generation[14,16] because the partial pressure of Sn in the gas phase is minimal. We are thus able to generate SnV^- centers with well-known plasma parameters typically used to grow pure diamond. The compatibility of SIIG with the standard growth conditions of the host material speaks to the versatility of the method. We believe that SIIG can be extended to other color centers in not only diamond but a multitude of other host materials[3] and may be of great use in new color center[36−38] discovery.

■ ASSOCIATED CONTENT

Supporting Information

The Supporting Information is available free of charge at https://pubs.acs.org/doi/10.1021/acs.nanolett.9b04495.

Experimental details and further discussions of inhomogeneous broadening, sample preparation, and conversion efficiency (PDF)

■ AUTHOR INFORMATION

Corresponding Author

Alison E. Rugar − *E. L. Ginzton Laboratory, Stanford University, Stanford, California 94305, United States;* orcid.org/0000-0002-7856-432X; Email: arugar@stanford.edu

Authors

Haiyu Lu − *Department of Physics and Geballe Laboratory for Advanced Materials, Stanford University, Stanford, California 94305, United States*

Constantin Dory − *E. L. Ginzton Laboratory, Stanford University, Stanford, California 94305, United States*

Shuo Sun − *E. L. Ginzton Laboratory, Stanford University, Stanford, California 94305, United States*

Patrick J. McQuade − *Department of Materials Science and Engineering, Stanford University, Stanford, California 94305, United States; Stanford Institute for Materials and Energy Sciences, SLAC National Accelerator Laboratory, Menlo Park, California 94025, United States*

Zhi-Xun Shen − *Department of Physics, Stanford University, Stanford, California 94305, United States; Stanford Institute for Materials and Energy Sciences, SLAC National Accelerator Laboratory, Menlo Park, California 94025, United States*

Nicholas A. Melosh − *Department of Materials Science and Engineering, Stanford University, Stanford, California 94305, United States; Stanford Institute for Materials and Energy Sciences, SLAC National Accelerator Laboratory, Menlo Park, California 94025, United States;* orcid.org/0000-0002-2601-1379

Jelena Vučković − *E. L. Ginzton Laboratory, Stanford University, Stanford, California 94305, United States*

Complete contact information is available at: https://pubs.acs.org/10.1021/acs.nanolett.9b04495

Notes

The authors declare no competing financial interest.

■ ACKNOWLEDGMENTS

This work was financially supported by the Army Research Office (ARO) (award no. W911NF-13-1-0309); the National Science Foundation (NSF) RAISE TAQS (award no. 1838976); the Air Force Office of Scientific Research (AFOSR) DURIP (award no. FA9550-16-1-0223); the Department of Energy, Basic Energy Sciences (BES)-Materials Science and Engineering; and SLAC LDRD. A.E.R. acknowledges support from the National Defense Science and Engineering Graduate (NDSEG) Fellowship Program, sponsored by the Air Force Research Laboratory (AFRL), the Office of Naval Research (ONR), and the Army Research Office (ARO). C.D. acknowledges support from the Andreas

https://dx.doi.org/10.1021/acs.nanolett.9b04495
Nano Lett. XXXX, XXX, XXX−XXX

Bechtolsheim Stanford Graduate Fellowship and the Microsoft Research Ph.D. Fellowship. Part of this work was performed at the Stanford Nanofabrication Facility (SNF) and the Stanford Nano Shared Facilities (SNSF), supported by the National Science Foundation under award ECCS-1542152.

REFERENCES

(1) Aharonovich, I.; Castelletto, S.; Simpson, D. A.; Su, C.-H.; Greentree, A. D.; Prawer, S. Diamond-based single-photon emitters. *Rep. Prog. Phys.* **2011**, *74*, 076501.
(2) Atatüre, M.; Englund, D.; Vamivakas, N.; Lee, S. Y.; Wrachtrup, J. Material platforms for spin-based photonic quantum technologies. *Nat. Rev. Mater.* **2018**, *3*, 38−51.
(3) Awschalom, D. D.; Hanson, R.; Wrachtrup, J.; Zhou, B. B. Quantum technologies with optically interfaced solid-state spins. *Nat. Photonics* **2018**, *12*, 516−27.
(4) Bradac, C.; Gao, W.; Forneris, J.; Trusheim, M.; Aharonovich, I. arXiv:1906.10992.
(5) Sipahigil, A.; Jahnke, K. D.; Rogers, L. J.; Teraji, T.; Isoya, J.; Zibrov, A. S.; Jelezko, F.; Lukin, M. D. Indistinguishable Photons from Separated Silicon-Vacancy Centers in Diamond. *Phys. Rev. Lett.* **2014**, *113*, 113602.
(6) Sukachev, D. D.; Sipahigil, A.; Nguyen, C. T.; Bhaskar, M. K.; Evans, R. E.; Jelezko, F.; Lukin, M. D. Silicon-Vacancy Spin Qubit in Diamond: A Quantum Memory Exceeding 10 ms with Single-Shot State Readout. *Phys. Rev. Lett.* **2017**, *119*, 223602.
(7) Sohn, Y.-I.; et al. Controlling the coherence of a diamond spin qubit through its strain environment. *Nat. Commun.* **2018**, *9*, 2012.
(8) Nguyen, C. T.; Sukachev, D. D.; Bhaskar, M. K.; Machielse, B.; Levonian, D. S.; Knall, E. N.; Stroganov, P.; Riedinger, R.; Park, H.; Lončar, M.; Lukin, M. D. Quantum Network Nodes Based on Diamond Qubits with an Efficient Nanophotonic Interface. *Phys. Rev. Lett.* **2019**, *123*, 183602.
(9) Nguyen, C. T.; Sukachev, D. D.; Bhaskar, M. K.; Machielse, B.; Levonian, D. S.; Knall, E. N.; Stroganov, P.; Chia, C.; Burek, M. J.; Riedinger, R.; Park, H.; Lončar, M.; Lukin, M. D. An integrated nanophotonic quantum register based on silicon-vacancy spins in diamond. *Phys. Rev. B: Condens. Matter Mater. Phys.* **2019**, *100*, 165428.
(10) Bayn, I.; Chen, E. H.; Trusheim, M. E.; Li, L.; Schröder, T.; Gaathon, O.; Lu, M.; Stein, A.; Liu, M.; Kisslinger, K.; Clevenson, H.; Englund, D. Generation of Ensembles of Individually Resolvable Nitrogen Vacancies Using Nanometer-Scale Apertures in Ultrahigh-Aspect Ratio Planar Implantation Masks. *Nano Lett.* **2015**, *15*, 1751−8.
(11) Schröder, T.; Trusheim, M. E.; Walsh, M.; Li, L.; Zheng, J.; Schukraft, M.; Sipahigil, A.; Evans, R. E.; Sukachev, D. D.; Nguyen, C. T.; Pacheco, J. L.; Camacho, R. M.; Bielejec, E. S.; Lukin, M. D.; Englund, D. Scalable focused ion beam creation of nearly lifetime-limited single quantum emitters in diamond nanostructures. *Nat. Commun.* **2017**, *8*, 15376.
(12) Zhou, Y.; Mu, Z.; Adamo, G.; Bauerdick, S.; Rudzinski, A.; Aharonovich, I.; bo Gao, W. Direct writing of single germanium vacancy center arrays in diamond. *New J. Phys.* **2018**, *20*, 125004.
(13) Crane, M. J.; Petrone, A.; Beck, R. A.; Lim, M. B.; Zhou, X.; Li, X.; Stroud, R. M.; Pauzauskie, P. J. High-pressure, high-temperature molecular doping of nanodiamond. *Sci. Adv.* **2019**, *5*, No. eaau6073.
(14) Neu, E.; Steinmetz, D.; Riedrich-Möller, J.; Gsell, S.; Fischer, M.; Schreck, M.; Becher, C. Single photon emission from silicon-vacancy colour centres in chemical vapour deposition nano-diamonds on iridium. *New J. Phys.* **2011**, *13*, 025012.
(15) Palyanov, Y. N.; Kupriyanov, I. N.; Borzdov, Y. M.; Surovtsev, N. V. Germanium: a new catalyst for diamond synthesis and a new optically active impurity in diamond. *Sci. Rep.* **2015**, *5*, 14789.
(16) Iwasaki, T.; et al. Germanium-Vacancy Single Color Centers in Diamond. *Sci. Rep.* **2015**, *5*, 12882.
(17) Thiering, G.; Gali, A. *Ab Initio* Magneto-Optical Spectrum of Group-IV Vacancy Color Centers in Diamond. *Phys. Rev. X* **2018**, *8*, 021063.
(18) Iwasaki, T.; Miyamoto, Y.; Taniguchi, T.; Siyushev, P.; Metsch, M. H.; Jelezko, F.; Hatano, M. Tin-Vacancy Quantum Emitters in Diamond. *Phys. Rev. Lett.* **2017**, *119*, 253601.
(19) Görlitz, J.; Herrmann, D.; Thiering, G.; Fuchs, P.; Gandil, M.; Iwasaki, T.; Taniguchi, T.; Kieschnick, M.; Meijer, J.; Hatano, M.; Gali, A.; Becher, C. Spectroscopic investigations of negatively charged tin-vacancy centres in diamond. *New J. Phys.* **2020**, *22*, 013048.
(20) Ekimov, E. A.; Lyapin, S. G.; Kondrin, M. V. Tin-vacancy color centers in micro- and polycrystalline diamonds synthesized at high pressures. *Diamond Relat. Mater.* **2018**, *87*, 223−7.
(21) Dobrinets, I.; Vins, V. G.; Zaitsev, A. *HPHT-Treated Diamonds*; Springer Series in Materials Science: Springer: Berlin, 2013; Chapter 5, Vol. *181*.
(22) Rugar, A. E.; Dory, C.; Sun, S.; Vučković, J. Characterization of optical and spin properties of single tin-vacancy centers in diamond nanopillars. *Phys. Rev. B: Condens. Matter Mater. Phys.* **2019**, *99*, 205417.
(23) Trusheim, M. E.; et al.et al Transform-Limited Photons From a Coherent Tin-Vacancy Spin in Diam. *Phys. Rev. Lett.* **2020**, *124*, 023602.
(24) Tchernij, S. D.; Herzig, T.; Forneris, J.; Küpper, J.; Pezzagna, S.; Train, P.; Morev, E.; Brida, I. P. D. G.; Skukan, N.; Genovese, M.; Jakšić, M.; Meijer, J.; Olivero, P. Single-Photon-Emitting Optical Centers in Diamond Fabricated upon Sn Implantation. *ACS Photonics* **2017**, *4*, 2580−2586.
(25) See the Supporting Information.
(26) Evans, R. E.; Sipahigil, A.; Sukachev, D. D.; Zibrov, A. S.; Lukin, M. D. Narrow-Linewidth Homogeneous Optical Emitters in Diamond Nanostructures via Silicon Ion Implantation. *Phys. Rev. Appl.* **2016**, *5*, 044010.
(27) Evans, R. E.; Bhaskar, M. K.; Sukachev, D. D.; Nguyen, C. T.; Sipahigil, A.; Burek, M. J.; Machielse, B.; Zhang, G.; Zibrov, A. S.; Bielejec, E.; Park, H.; Lončar, M.; Lukin, M. D. Photon-mediated interactions between quantum emitters in a diamond nanocavity. *Science* **2018**, *362*, 662−5.
(28) Sipahigil, A.; et al. An integrated diamond nanophotonics platform for quantum-optical networks. *Science* **2016**, *354*, 847−50.
(29) Sun, S.; Zhang, J. L.; Fischer, K. A.; Burek, M. J.; Dory, C.; Lagoudakis, K. G.; Tzeng, Y.-K.; Radulaski, M.; Kelaita, Y.; Safavi-Naeini, A.; Shen, Z.-X.; Melosh, N. A.; Chu, S.; Lončar, M.; Vučković, J. Cavity-Enhanced Raman Emission from a Single Color Center in a Solid. *Phys. Rev. Lett.* **2018**, *121*, 083601.
(30) Burek, M. J.; Chu, Y.; Liddy, M. S. Z.; Patel, P.; Rochman, J.; Meesala, S.; Hong, W.; Quan, Q.; Lukin, M. D.; Lončar, M. High quality-factor optical nanocavities in bulk single-crystal diamond. *Nat. Commun.* **2014**, *5*, 5718.
(31) Khanaliloo, B.; Mitchell, M.; Hryciw, A. C.; Barclay, P. E. High-Q/V Monolithic Diamond Microdisks Fabricated with Quasiisotropic Etching. *Nano Lett.* **2015**, *15*, 5131−6.
(32) Mouradian, S.; Wan, N. H.; Schröder, T.; Englund, D. Rectangular photonic crystal nanobeam cavities in bulk diamond. *Appl. Phys. Lett.* **2017**, *111*, 021103.
(33) Wan, N. H.; Mouradian, S.; Englund, D. Two-dimensional photonic crystal slab nanocavities on bulk single-crystal diamond. *Appl. Phys. Lett.* **2018**, *112*, 141102.
(34) Mitchell, M.; Lake, D. P.; Barclay, P. E. Realizing Q 300 000 in diamond microdisks for optomechanics via etch optimization. *APL Photonics* **2019**, *4*, 016101.
(35) Dory, C.; Vercruysse, D.; Yang, K. Y.; Sapra, N. V.; Rugar, A. E.; Sun, S.; Lukin, D. M.; Piggott, A. Y.; Zhang, J. L.; Radulaski, M.; Lagoudakis, K. G.; Su, L.; Vučković, J. Inverse-designed diamond photonics. *Nat. Commun.* **2019**, *10*, 3309.
(36) Trusheim, M. E.; Wan, N. H.; Chen, K. C.; Ciccarino, C. J.; Flick, J.; Sundararaman, R.; Malladi, G.; Bersin, E.; Walsh, M.; Lienhard, B.; Bakhru, H.; Narang, P.; Englund, D. Lead-related

https://dx.doi.org/10.1021/acs.nanolett.9b04495
Nano Lett. XXXX, XXX, XXX−XXX

quantum emitters in diamond. *Phys. Rev. B: Condens. Matter Mater. Phys.* **2019**, *99*, 075430.
(37) Tchernij, S. D.; et al. Single-Photon Emitters in Lead-Implanted Single-Crystal Diamond. *ACS Photonics* **2018**, *5*, 4864−4871.
(38) Harris, I.; Ciccarino, C. J.; Flick, J.; Englund, D. R.; Narang, P. arXiv:1907.12548.

https://dx.doi.org/10.1021/acs.nanolett.9b04495
Nano Lett. XXXX, XXX, XXX−XXX